Visualizing Nonlinear Vector Field Topology

Gerik Scheuermann, Heinz Krüger, Martin Menzel, and Alyn P. Rockwood

Abstract—We present our results on the visualization of nonlinear vector field topology. The underlying mathematics is done in Clifford algebra, a system describing geometry by extending the usual vector space by a multiplication of vectors. We started with the observation that all known algorithms for vector field topology are based on piecewise linear or bilinear approximation, and that these methods destroy the local topology if nonlinear behavior is present. Our algorithm looks for such situations, chooses an appropriate polynomial approximation in these areas, and, finally, visualizes the topology. This overcomes the problem, and the algorithm is still very fast because we are using linear approximation outside these small but important areas. The paper contains a detailed description of the algorithm and a basic introduction to Clifford algebra.

Index Terms—Vector field topology, Clifford algebra, visualization.

———————————— ✦ ————————————

1 INTRODUCTION

T HE topology of vector fields has received a lot of attention in the visualization community since its introduction by Helman and Hesselink [5], [6]. One reason is its capability to reduce the amount of information in the field so that an understanding of the whole structure becomes possible. All algorithms start with a piecewise linear or bilinear interpolation of the data at certain grid positions. Then, one looks for all the saddle points and starts the numerical computation of the separatrices from there. One gets a graph with vertices at the zeros and separatrices as edges which is called topological skeleton.

The problem we faced with this method is the fact that the piecewise linear or bilinear interpolation destroys the topology if there are higher-order singularities or close critical points present. This can also affect the global topology by destroying elliptic sectors where the integration curves tend back to their starting point. Our solution is based on the idea that the local approximation of the field has to depend on the possible local topological structure. We look at the linear approximation and check if nonlinear local behavior is present, especially higher-order singularities. If present, we choose a polynomial approximation of suitable degree in this area to be able to detect the nonlinear behavior. If not, we just keep the linear approximation of the vector field. This keeps the algorithm fast, because, in typical applications, one will not have nonlinear local behavior in most grid cells.

We think that [14] was the first paper dealing with the visualization of higher-order singularities. In the next sec-

tion we describe some of the changes in the topology in this case. There is also an example which has been visualized by a nice program from Bhinderwala [2]. A different interesting aspect of the topology of vector fields is the relation between the Euler characteristic of the space and the indices of the singularities in the vector fields given by the Poincaré-Hopf theorem in Section 3.

The polynomial approximation is based on results about the Clifford algebra description of vector fields. Because this is a nearly unknown subject in the computer graphics and visualization community, we give a basic introduction in two sections. This knowledge is then used to show new results about vector fields which have been proven partly in [15]. These new insights opened the way for an algorithm dealing with higher-order singularities. It starts with a piecewise linear interpolated unstructured grid and looks for regions with close singularities. Then, the approximation in these regions is replaced by a polynomial approximation of sufficient degree to model possible higher-order singularities. Finally, the resulting topological graph is visualized with an extension of the usual algorithm. The last section gives some examples and shows aspects of nonlinear behavior.

2 VECTOR FIELD TOPOLOGY

The question in vector field topology is the qualitative behavior of the integration curves. The theory was introduced by Poincaré at the end of the last century after his observation that a direct computation of the solution curves by power series may fail [12], [13]. The easiest curve is just a point occurring at a zero in the vector field. These points are also called critical points. To understand their role in the field, one looks at their Poincaré-index or winding number. It counts the number of turns of the field around the zero as can be seen in Fig. 1 in the case of a saddle point.

Most of the other integration curves start at such positions and tend to other critical points or the boundary. If one can continuously transform one curve into another curve, one says that these two curves have the same qualitative structure. The basic idea is now to find regions of the

- G. Scheuermann is with the FB Informatik, Universität Kaiserslautern, Postfach 3049, 67653 Kaiserslautern, Germany.
  E-mail: scheuer@informatik.uni-kl.de.
- H. Krüger and M. Menzel are with the FB Physik, Universität Kaiserslautern, Postfach 3049, 67653 Kaiserslautern, Germany.
  E-mail: krueger@physik.uni-kl.de, menzel@physicist.net.
- A.P. Rockwood is with the Department of Computer Science and Engineering, College of Engineering and Applied Sciences, Arizona State University, Box 875406, Tempe, AZ 85287-5406.
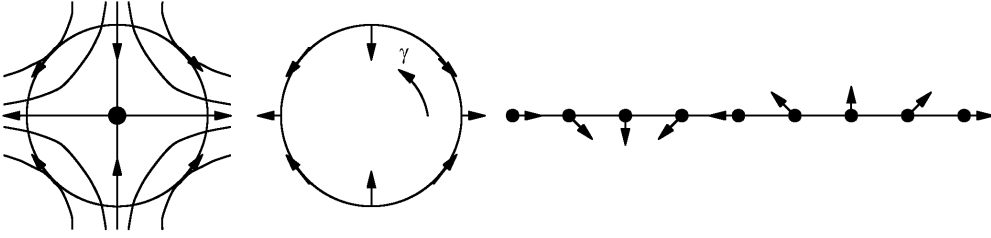 E-mail: rockwood@asu.edu.

Fig. 1. Winding number of a saddle point.

same qualitative behavior, called basins. In a 2D vector field, the border of a basin consists of integration curves which are called separatrices. One can find them by looking for curves starting at the saddle points if only simple critical points are present.

If higher-order critical points are present, one has to do a little bit more, but the procedure is similar. The separatrices now start at points with negative index, and these points are sometimes called higher-order saddles. In our polynomial case, there are again only a finite number of them, so one can still draw them. Fig. 2 may now illustrate the topology with higher-order local behavior. The separatrices starting at the monkey saddle are in light blue and the other separatrices appear darker to show the effect of the separatrices starting at this point of higher negative index in the field topology.

3 SPACE TOPOLOGY AND VECTOR FIELDS

The possible topology of a vector field depends on topological properties of the manifold where it is defined. This section introduces the necessary topological definitions and results. For a more detailed description, one may look into [10].

A topological space X homeomorphic to the interior $\dot{D}^n$ of the unit disc is called an n-cell. One looks for a decomposition of the whole space into such elements.

A cellular decomposition of a manifold X is a set of subspaces of X with the following properties:

1) $X = \bigcup_{e \in C} e$ and $e \cap e' = \varnothing$ for $e \neq e'$
2) Every $e \in C$ is an $|e|$-cell, $|e| \in \mathbb{N}$.
3) For each $e \in C$, there exists a map $\phi_e : D^n \to X$, $n = |e|$, so that $\phi_e | \dot{D}^n$ is a homeomorphism of $\dot{D}^n$ and e and
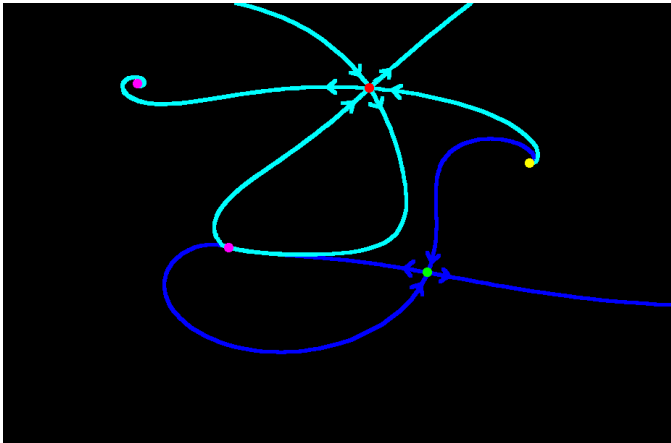
$$\phi_e(S^{n-1}) \subset X^{n-1} := \bigcup_{e' \in C, |e'| \leq n-1} e'.$$

X^{n-1} is called $(n-1)$-skeleton of the cellular decomposition.

Such a cellular decomposition is called CW-decomposition if

(C) for every $e \in C$ is $\bar{e}$ a subset of a finite union of cells in C.

(W) A subset $A \subset X$ is closed if and only if $A \cap \bar{e}$ is closed in $\bar{e}$ $\forall e \in C$.

Fig. 3 gives an example for a torus.
The Euler characteristic $\chi(X)$ of X is then defined as

$$\chi(X) = \sum_{q=0}^{\infty} (-1)^q \alpha_q, \tag{1}$$

where α_q is the number of q-cells in X. The Euler characteristic does not depend on the CW-decomposition.

A connection between the indices of a vector field and the Euler characteristic of the manifold is given by the following theorem.

THEOREM 1 (Poincaré-Hopf). *Let* M *be a compact oriented n-manifold and* $v : M \to TM$ *a smooth vector field with isolated zeros. The sum of the indices at the zeros equals the Euler characteristic of* M:

$$\sum_{\substack{z \in M \\ v(z) = 0}} ind_z = \chi(M) \tag{2}$$

PROOF. [17, pp. 35-41].   □

Fig. 2. Topology with higher-order local behavior.

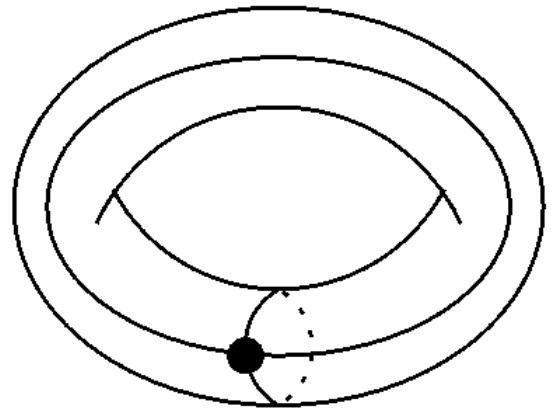

Fig. 3. CW-decomposition of a torus.

4 CLIFFORD ALGEBRA

Clifford algebra is a way to extend the usual description of geometry by a multiplication of vectors. We give a basic introduction in the two-dimensional case, but it can be done in any dimension.

We start with a usual vector $v \in R^2$. Together with the Euclidean standard basis $\{e_1, e_2\}$, it can be written as

$$v = v_1 e_1 + v_2 e_2. \tag{3}$$

The standard description as a column vector gives

$$v = v_1 \begin{pmatrix} 1 \\ 0 \end{pmatrix} + v_2 \begin{pmatrix} 0 \\ 1 \end{pmatrix}$$
$$= \begin{pmatrix} v_1 \\ v_2 \end{pmatrix}. \tag{4}$$

If we would use square matrices instead, we could take

$$v = v_1 \begin{pmatrix} 0 & 1 \\ 1 & 0 \end{pmatrix} + v_2 \begin{pmatrix} 1 & 0 \\ 0 & -1 \end{pmatrix}$$
$$= \begin{pmatrix} v_2 & v_1 \\ v_1 & -v_2 \end{pmatrix}. \tag{5}$$

This looks a little bit strange, but it allows a matrix multiplication of vectors.

$$vw = \begin{pmatrix} v_2 & v_1 \\ v_1 & -v_2 \end{pmatrix} \begin{pmatrix} w_2 & w_1 \\ w_1 & -w_2 \end{pmatrix}$$
$$= \begin{pmatrix} v_1 w_1 + v_2 w_2 & v_2 w_1 - v_1 w_2 \\ v_1 w_2 - v_2 w_1 & v_1 w_1 + v_2 w_2 \end{pmatrix}. \tag{6}$$

With a suitable choice of the remaining two basis vectors of the square matrices, we get

$$vw = (v_1 w_1 + v_2 w_2) \begin{pmatrix} 1 & 0 \\ 0 & 1 \end{pmatrix} +$$
$$(v_1 w_2 - v_2 w_1) \begin{pmatrix} 0 & -1 \\ 1 & 0 \end{pmatrix}. \tag{7}$$

With the terms

$$1 := \begin{pmatrix} 1 & 0 \\ 0 & 1 \end{pmatrix} \quad i := \begin{pmatrix} 0 & -1 \\ 1 & 0 \end{pmatrix}, \tag{8}$$

we end up with a four-dimensional algebra G_2 with the following rules for the multiplication

$$1 e_j = e_j \quad j = 1, 2 \tag{9}$$

$$e_j 1 = e_j \quad j = 1, 2 \tag{10}$$

$$1^2 = 1 \tag{11}$$

$$e_j^2 = 1 \quad j = 1, 2 \tag{12}$$

$$i^2 = -1 \tag{13}$$

$$e_1 e_2 = -e_2 e_1 = i. \tag{14}$$

The following projections are useful for computations

$$<\cdot>_0 : G_2 \to R \subset G_2$$
$$a1 + be_1 + ce_2 + di \mapsto a1 \tag{15}$$

$$<\cdot>_1 : G_2 \to R^2 \subset G_2$$
$$a1 + be_1 + ce_2 + di \mapsto be_1 + ce_2 \tag{16}$$

$$<\cdot>_0 : G_2 \to Ri \subset G_2$$
$$a1 + be_1 + ce_2 + di \mapsto di. \tag{17}$$

From (7), we also get for two vectors $v, w \in R^2 \subset G_2$

$$vw = (v \bullet w) + (v \wedge w), \tag{18}$$

where $\bullet$ is the usual scalar product and $\wedge$ the outer product of Grassmann. Now, we have got a unification of these two products into an associative multiplication.

In [16], one can find constructions like this one for every dimension n by using 2^n-dimensional subalgebras of a complex matrix algebra $Mat(m, C)$. These algebras are models for a Clifford algebra describing n-dimensional Euclidean space. More details can be found in the literature, [3], [7], [16].

In our 2D-case we have another important fact: Because of (13), one can interpret the elements

$$a1 + bi \in G_2 \tag{19}$$

of our algebra as the complex numbers, but with the unusual interpretation as scalars plus bivectors.

5 CLIFFORD ANALYSIS

After extending the structure of the linear algebra, one may also change the analysis. This leads especially to a differential operator that does not depend on the coordinates as we demonstrate below.

Our maps will be multivector fields

$$A : R^2 \to G_2$$
$$r \mapsto A(r). \tag{20}$$

A Clifford vector field is just a multivector field with values in $R^2 \subset G_2$

$$v : R^2 \to R^2 \subset G_2$$
$$xe_1 + ye_2 \mapsto v_1(x, y)e_1 + v_2(x, y)e_2. \tag{21}$$

The directional derivative of A in direction $b \in R^2$ is defined by

$$A_b(r) = \lim_{\epsilon \to 0} \frac{1}{\epsilon} [A(r + \epsilon b) - A(r)]. \tag{22}$$

This allows the definition of the vector derivative of A at $r \in R^2$

$$\partial A(r) : R^2 \to G_2$$
$$r \mapsto \partial A(r) = \sum_{k=1}^2 g^k A_{g_k}(r). \tag{23}$$

This is independent of the basis $\{g_1, g_2\}$ of R^2. The vectors

$$g^1 = \frac{i}{\gamma} g_2 \quad g^2 = \frac{i}{\gamma} g_1 \tag{24}$$

with

$$g_1 \wedge g_2 = \gamma i \tag{25}$$

are called reciprocal vectors.

For a vector field $v : R^2 \to R^2$, one gets, in Euclidean coordinates,

$$\partial v = \sum_{j=1}^{2} e_j v_{e_j}$$

$$= \sum_{j=1}^{2} e_j \left(\frac{\partial v_1}{\partial e_j} e_1 + \frac{\partial v_2}{\partial e_j} e_2 \right)$$

$$= \left(\frac{\partial v_1}{\partial e_1} + \frac{\partial v_2}{\partial e_2} \right) 1 + \left(\frac{\partial v_2}{\partial e_1} - \frac{\partial v_1}{\partial e_2} \right) i$$

$$\partial v = (\text{div } v) 1 + (\text{curl } v) i. \tag{26}$$

So, this differential operator integrates divergence and rotation.

The integral is defined as follows:

Let $M \subset R^2$ be an oriented r-manifold and $A, B : M \to R^2$ be two piecewise continuous multivector fields. Then, one defines the integral

$$\int_M A dX B \tag{27}$$

as the limit

$$\lim_{n \to \infty} \sum_{i=0}^{n} A(x_i) \Delta X(x_i) B(x_i), \tag{28}$$

where $\Delta X(x_i)$ is a r-volume in the usual Riemannian sense. This allows the definition of the Poincaré-index of a vector field v at $a \in R^2$ as

$$\text{ind}_a v = \lim_{\epsilon \to 0} \frac{1}{2\pi i} \int_{S_\epsilon^1} \frac{v \wedge dv}{v^2}, \tag{29}$$

where S_ϵ^1 is a circle of radius ϵ around a.

6 THEORETICAL RESULTS

For our analysis of vector fields, it is necessary to look at $v : R^2 \to R^2 \subset G_2$ in suitable coordinates. Let $z = x + iy$, $\bar{z} = x - iy$ be complex numbers in the algebra. This means

$$x = \frac{1}{2}(z + \bar{z}) \tag{30}$$

$$y = \frac{1}{2i}(z - \bar{z}). \tag{31}$$

We get

$$v(r) = v_1(x, y) e_1 + v_2(x, y) e_2$$

$$= \left[v_1\left(\frac{1}{2}(z + \bar{z}), \frac{1}{2i}(z - \bar{z}) \right) - \right.$$

$$\left. i v_2\left(\frac{1}{2}(z + \bar{z}), \frac{1}{2i}(z - \bar{z}) \right) \right] e_1$$

$$= E(z, \bar{z}) e_1, \tag{32}$$

where

$$E : C^2 \to C \subset G_2$$

$$(z, \bar{z}) \mapsto v_1\left(\frac{1}{2}(z + \bar{z}), \frac{1}{2i}(z - \bar{z}) \right)$$

$$- i v_2\left(\frac{1}{2}(z + \bar{z}), \frac{1}{2i}(z - \bar{z}) \right) \tag{33}$$

is a complex-valued function of two complex variables. The idea is now to analyze E instead of v and get topological results directly from the formulas in some interesting cases.

Let us first assume that E and v are linear.

THEOREM 2. *Let*

$$v(r) = (az + b\bar{z} + c) e_1 \tag{34}$$

be a linear vector field. For $|a| \neq |b|$, it has a unique zero at $z_0 e_1 \in R^2$. For $|a| > |b|$, has one saddle point with index -1. For $|a| < |b|$, it has one critical point with index 1. The special types in this case can be obtained from the following list:

1) $Re(b) = 0 \Leftrightarrow$ *circle at z_0.*
2) $Re(b) \neq 0$, $|a| > |Im(b)| \Leftrightarrow$ *node at z_0.*
3) $Re(b) \neq 0$, $|a| < |Im(b)| \Leftrightarrow$ *spiral at z_0.*
4) $Re(b) \neq 0$, $|a| = |Im(b)| \Leftrightarrow$ *focus at z_0.*

In Cases 2-4, one has a sink for $Re(b) < 0$ and a source for $Re(b) > 0$. For $|a| = |b|$, one gets a whole line of zeros.

PROOF. A computation of the derivatives of the components v_1, v_2 and a comparison with the well-known classification gives this result. □

We included this easy theorem to show that this description gives topological information more directly. Let us look now at the general polynomial case.

THEOREM 3. *Let $v : R^2 \to R^2 \subset G_2$ be an arbitrary polynomial vector field with isolated critical points. Let $E : C^2 \to C$ be the polynomial, so that $v(r) = E(z, \bar{z}) e_1$. Let $F_k : C^2 \to C$, $k = 1, \ldots, n$ be the irreducible components of E, so that $E(z, \bar{z}) = \prod_{k=1}^{n} F_k$. Then, the vector fields $w_k : R^2 \to R^2$, $w_k(r) = F_k(r) e_1$ have only isolated zeros $z_1, \ldots, z_m$. These are then the zeros of v and for the Poincaré-indices we have*

$$\text{ind}_{z_j} v = \sum_{k=1}^{n} \text{ind}_{z_j} w_k. \tag{35}$$

PROOF. The w_k have only isolated zeros because, otherwise, v would also have no isolated zeros. It is also obvious that a zero of a w_k is a zero of v and a zero of v must be a zero of one of the w_k.

For the derivatives, we get

$$\frac{\partial E}{\partial z} = a \sum_{k=1}^{n} \frac{\partial F_k}{\partial z} \prod_{l=1, l \neq k}^{n} F_l \tag{36}$$

$$\frac{\partial E}{\partial \bar{z}} = a \sum_{k=1}^{n} \frac{\partial F_k}{\partial \bar{z}} \prod_{l=1, l \neq k}^{n} F_l. \tag{37}$$

For the computation of the Poincaré-index, we assume $z_j = 0$ after a change of the coordinate system and that ϵ is so small that there are no other zeros inside S_ϵ^1. We get

$$\mathrm{ind}_{z_j} v = \frac{1}{2\pi i} \int_{S_\varepsilon^1} \frac{v \wedge dv}{v^2}$$

$$= \frac{1}{2\pi i} \int_{S_\varepsilon^1} \frac{1}{v^2} < a\prod_{k=1}^n F_k e_1 \left[dz\; a\sum_{k=1}^n \frac{\partial F_k}{\partial z} \prod_{l=1, l\neq k}^n F_l + d\bar{z}\; a\sum_{k=1}^n \frac{\partial F_k}{\partial \bar{z}} \prod_{l=1, l\neq k}^n F_l \right] e_1 >_2$$

$$= \frac{1}{2\pi i} \int_{S_\varepsilon^1} \frac{1}{v^2} < a\bar{a}\sum_{k=1}^n F_k \overline{\left(dz\frac{\partial F_k}{\partial z} + d\bar{z}\frac{\partial F_k}{\partial \bar{z}} \right)} \prod_{l=1, l\neq k}^n F_l \bar{F}_l >_2$$

$$= \sum_{k=1}^n \frac{1}{2\pi i} \int_{S_\varepsilon^1} \frac{1}{F_k \bar{F}_k} < F_k e_1 \left(dz\frac{\partial F_k}{\partial z} + d\bar{z}\frac{\partial F_k}{\partial \bar{z}} \right) e_1 >_2$$

$$= \sum_{k=1}^n ind_{z_j} F_k e_1$$

$$= \sum_{k=1}^n ind_{z_j} w_k.$$

$\square$

The algorithm uses linear factors because of their simple behavior, as described in Theorem 2.

THEOREM 4. *Let* $v : R^2 \rightarrow R^2 \subset G_2$ *be the vector field* $v(r) = E(z, \bar{z})e_1$ *with*

$$E(z, \bar{z}) = \prod_{k=1}^n \left(a_k z + b_k \bar{z} + c_k \right), \qquad (38)$$

$|a_k| \neq |b_k|$ *and let* z_k *be the unique zero of* $a_k z + b_k \bar{z} + c_k$. *Then, v has zeros at* z_j, $j = 1, \ldots, n$ *and the Poincaré index of v at* z_j *is the sum of the indices of the* $(a_k z + b_k \bar{z} + c_k)e_1$ *at* z_j.

PROOF. Special case of Theorem 3. $\square$

7 THE ALGORITHM

This section shows a way for the visualization of nonlinear vector field topology.

Our central point is that, in conventional approaches, each grid cell contains a linear or bilinear vector field and cannot model a nonlinear local behavior. This can be seen in an unstructured grid consisting of triangles. If one approximates the triangles by linear interpolation, each triangle only contains one critical point but, in reality, there may be more inside. The key for a solution is to analyze the data to extract information about the number and index of critical points and to choose an approximation in the light of the theorems to allow several critical points if necessary. Outside the areas with more than one critical point, we use linear interpolation to keep the algorithm fast.

The basic idea is that a critical point has topological implications into the field if its Poincaré index is different from zero. The effect of the piecewise linear behavior can be seen in Fig. 4. There is a monkey saddle in one triangle, but, in a piecewise linear approximation, there will be two different triangles containing one saddle each.

This example tells how to find such situations. If several critical points are in the same cell and have the same index, one will notice close cells with critical points of that index in the linear approach. These areas are found in the first step and, then, we approximate with polynomials like the ones in the last section. In our example above, one could use
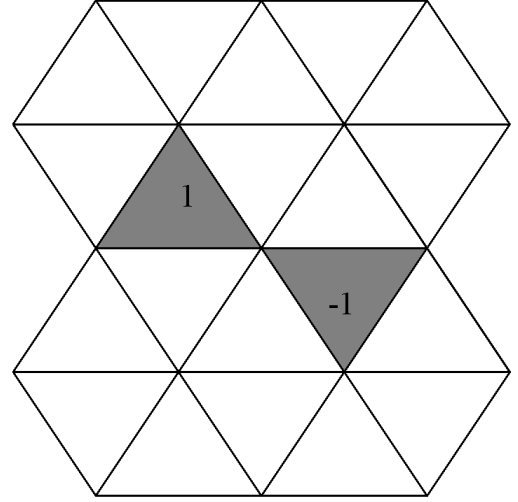

Fig. 4. Indices of triangles around a triangle with two saddles.

$$v(r) = \left(a_1 z + b_1 \bar{z} + c_1 \right)\left(a_2 z + b_2 \bar{z} + c_2 \right)e_1 \qquad (39)$$

in this area and, then, one can get the saddles in the same triangle.

Our algorithm includes, therefore, the following steps for finding the appropriate approximation:

1) Compute the Poincaré index around each triangle assuming linear interpolation along the edges. One gets −1, 0, or +1.

2) Build the regions of close triangles with possible higher-order critical points.

   a) If there are two triangles with a common edge and opposite index as in Fig. 5, mark them and save the neighboring connection.

   b) If there are unmarked triangles with the same index and a common vertex, put all the triangles with that vertex in a region as in Fig. 6. If one of the triangles is marked in a), put its neighbor in the region as in Fig. 7. If any of the triangles is already in a region, do not build this region. Otherwise, mark all the triangles in this new region.

   c) If there are unmarked triangles A and B with the same index and a triangle C with a common edge with A and a common vertex V with B as in Fig. 8, build a region consisting of A and all the triangles having V as vertex. Similar to b), we look for triangles which have been marked in a) and always put the neighbors in the region. Again, if any triangle in this new region is already in a region, do not build this region.

3) Compute the index of each region by just adding the index of all triangles in that region. Then, set up a polynomial approximation of the type

$$v(r) = \left(a_1 z + b_1 \bar{z} + c_1 \right) * \left(a_2 z + b_2 \bar{z} + c_2 \right) *$$
$$\ldots * \left(a_n z + b_n \bar{z} + c_n \right)e_1. \qquad (40)$$

Outside the regions from Step (2) ,we just do linear approximation of each triangle, so there is no change to the conventional algorithm. The remaining steps consist of
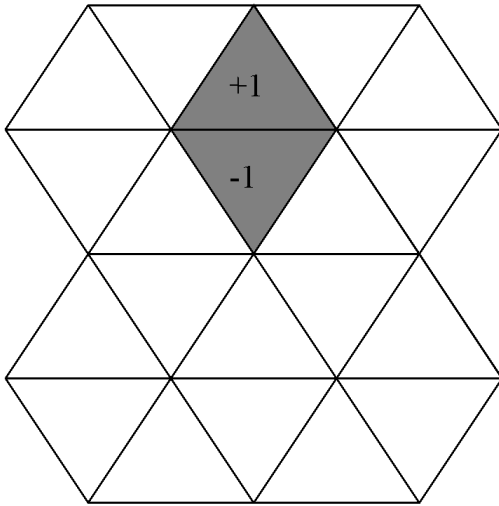
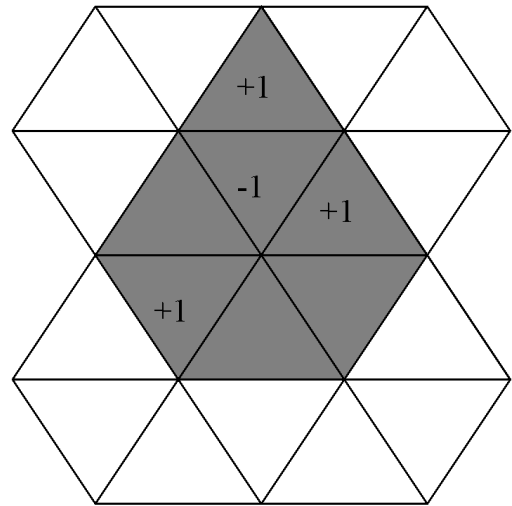Fig. 5. Triangles with opposite indices.
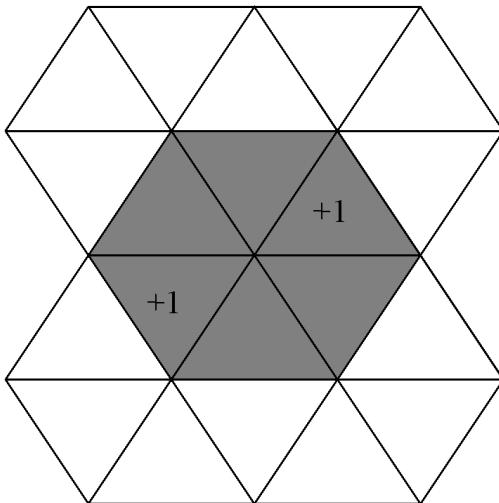

Fig. 7. A +2-region with +1/–1-pair.

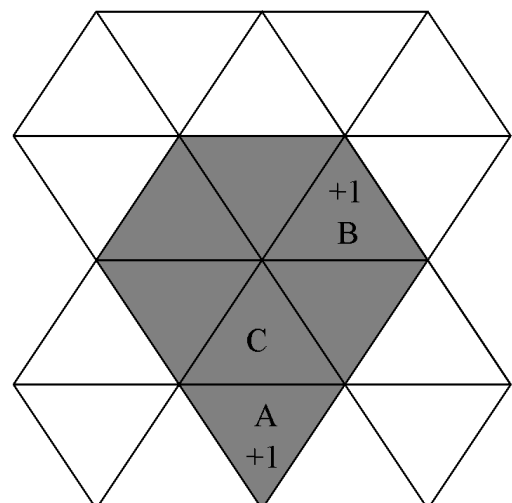Fig. 6. A region with two triangles having positive index.

Fig. 8. A more complicated region.

finding the critical points and separatrices and, finally, visualizing the topological graphs like the figures in the examples.

We are not maintaining continuity across the boundaries at the moment, but are thinking about some kind of blending in an area close to the boundary of our regions to solve this problem.

8 EXAMPLES

This section gives four examples of the algorithm. There are always several simple critical points together with higher-order critical points showing nonlinear behavior in the field.

The first example shows a monkey saddle together with three sinks and two saddles in Fig. 9. The data is given on a 40×40 quadratic grid which has been triangulated prior to the algorithm. It is a rather simple example with some nonlinear behavior present.

Fig. 10 contains the second example with two dipoles, a monkey saddle, and four simple critical points. The upper

right corner shows two elliptic sectors of the dipole where the integration curves go back to the dipole. This kind of global nonlinear behavior does not appear in piecewise linear fields, where no integration curve goes back to the critical point where it started. Around the monkey saddle, one can see some artifacts in the separatrices which come from the boundary between the piecewise linear outside and the polynomial approximation around the monkey saddle. This kind of artifact is one of the problems where further research is necessary. The topological graph shows how the higher-order singularities fit into the well-known connections between the simple critical points. The data was again given on a 40×40 quadratic grid.

In the third example in Fig. 11, there are 14 critical points. Twelve points are of linear type and two of higher-order. We have an elliptic sector below the dipole showing nonlinear behavior. The artifacts in the separation curve near the dipole are due to the boundary between polynomial and linear approximation.

The last example in Fig. 12 shows two dipoles surrounded by four saddle points and a source. There are four
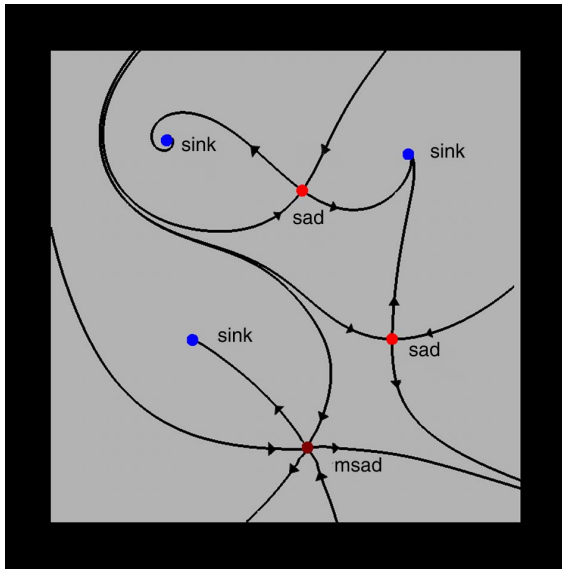
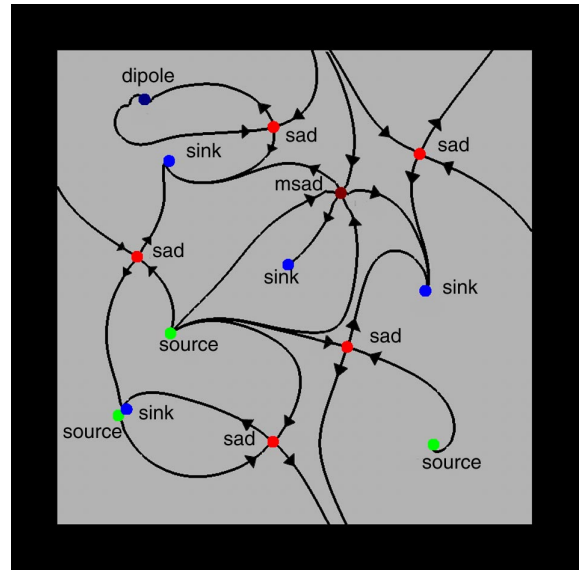Fig. 9. A monkey saddle with several simple critical points.
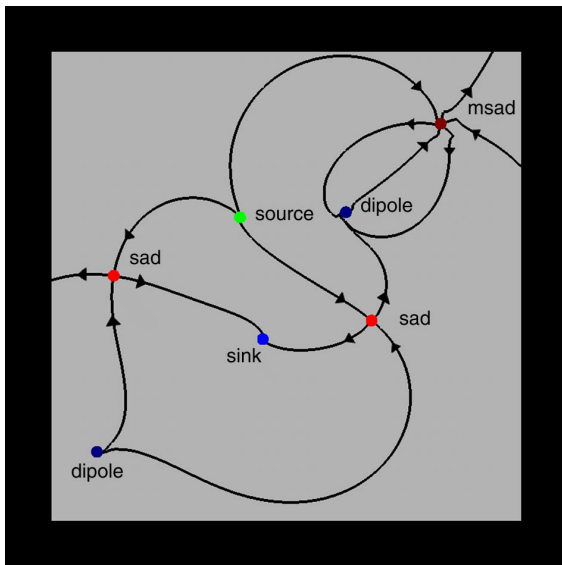

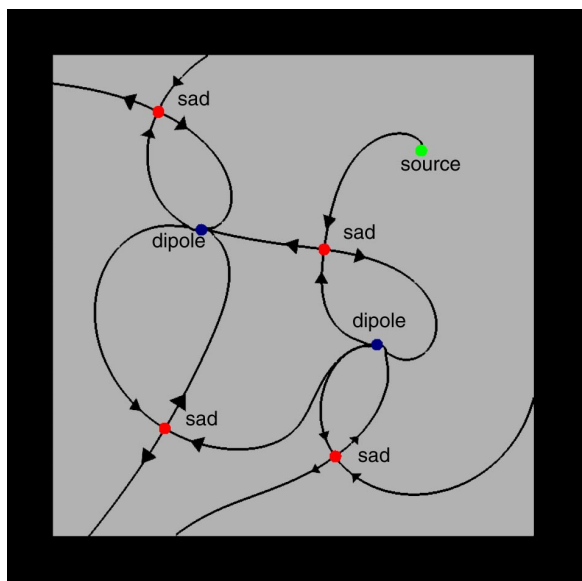Fig 11. Fourteen critical points.

Fig. 10. Seven critical points.

Fig. 12. Two interacting dipols with five simple critical points.

elliptic sectors and one can see that all the separatrices tend to dipoles along a common line similar to the theoretical examples in [14]. We used a 40×40 quadratic grid for the data.

9 CONCLUSION

We have presented an extension of our algorithm for the visualization of nonlinear vector field topology. It is based on the tight relation between topology and Clifford vector field description which is proved in the paper. The key idea is using a polynomial approximation with sufficient degree in regions of possible nonlinear behavior.

The whole article discusses two-dimensional problems, so the question about three-dimensional problems arises. A solution will be subject to further research, but it will take time. One reason is the qualitatively different behavior of such flows.

REFERENCES

[1]   V.I. Arnold, *Ordinary Differential Equations*. Berlin: Springer, 1992.
[2]   S.A. Bhinderwala, "Design and Visualization of Vector Fields," master's thesis, Arizona State Univ., 1997.
[3]   J.E. Gilbert and M.A.M. Murray, *Clifford Algebras and Dirac Operators in Harmonic Analysis*. Cambridge, U.K.: Cambridge Univ. Press, 1991.
[4]   J. Guckenheimer and P. Holmes, *Dynamical Systems and Bifurcation of Vector Fields*. New York: Springer, 1983.
[5]   J.L. Helman and L. Hesselink, "Surface Representations of Two- and Three-Dimensional Fluid Flow Topology," *Visualization in Scientific Computing*, G.M. Nielson and B. Shriver, eds., pp. 6-13. Los Alamitos, Calif.: IEEE CS Press, 1990.
[6]   J.L. Helman and L. Hesselink, "Visualizing Vector Field Topology in Fluid Flows," *IEEE Computer Graphics and Applicaitons*, vol. 11, no. 3, pp. 36-46, May 1991.
[7]   D. Hestenes, *New Foundations for Classical Mechanics*. Dordrecht: Kluwer Academic, 1986.
[8]   M.W. Hirsch and S. Smale, *Differential Equations, Dynamical Systems and Linear Algebra*. New York: Academic Press, 1974.
[9]   H. Krüger and M. Menzel, "Clifford-Analytic Vector Fields as Model for Plane Electric Currents," *Analytical and Numerical Methods in Quaternionic and Clifford Analysis*, W. Sprössig and K. Gürlebeck, eds., pp. 101-111. Seiffen, 1996.
[10] J.W. Milnor, *Topology from the Differential Viewpoint*. Charlottesville, Va.: The Univ. Press of Virginia, 1965.
[11] G.M. Nielson, I.-H. Jung, and J. Sung, "Haar Wavelets Over Triangular Domains With Applications to Multiresolution Models for Flow Over a Sphere," *Proc. IEEE Visualization '97*, pp. 143-149, Phoenix, Ariz., 1997.
[12] H. Poincaré, *Mémoire sur les cóurbes définés par les équations différentielles I-IV*. Paris: Gauthier-Villar, 1880-1890.
[13] H. Poincaré, "Sur les équations de la dynamique et le problème de trois corps," *Acta Mathematica*, vol. 13, pp. 1-270, 1890.
[14] G. Scheuermann, H. Hagen, H. Krüger, M. Menzel, and A. Rockwood, "Visualization of Higher-order Singularities in Vector Fields," *Proc. IEEE Visualization '97*, pp. 67-74, Los Angeles, 1997.
[15] G. Scheuermann, H. Hagen, and H. Krüger, "An Interesting Class of Polynomial Vector Fields," *Mathematical Methods for Curves and Surfaces II*, M. Dæhlen, T. Lyche, and L.L. Schumaker, eds., pp. 429-436, Nashville, Tenn., 1998.
[16] J. Snygg, *Clifford Algebra: A Computational Tool for Physicists*. Oxford: Oxford Univ. Press, 1997.
[17] R. Stoecker and H. Zieschang, *Algebraische Topologie*. Stuttgart: Teubner, 1994.
[18] F. Verhulst, *Nonlinear Differential Equations and Dynamical Systems*. Berlin: Springer, 1990.

Gerik Scheuermann studied mathematics and computer science from 1989-1995 at the Universität Kaiserslautern. In 1995, he received a diplom in mathematics. His diploma thesis concerned the construction and computation of moduli spaces for modules over curve singularities. Since 1996, he has been a research assistant in the Department of Computer Science at the Universität Kaiserslautern. In 1995 and 1996, he made three research visits to Arizona State University to perform parts of this work.

His research interests include algebraic geometry, topology, Clifford algebra, and scientific visualization.

Heinz Krüger studied physics and mathematics from 1960-1965 in Freiburg, where he received his diplom in theoretical physics at the end of 1965. From 1965-1968, he worked on his doctoral thesis in theoretical physics. In 1968, he finished his doctor's degree. From 1969 until 1972, he held a permanent position as a research assistant at the Max-Planck-Institut, Göttingen, in the section of atomic and molecular physics. In 1972, he became a professor of theoretical physics at the Universität Kaiserslautern. He is a member of the Comité Scientifique de la Fondation Louis de Broglie, Paris.

His research interests concern Clifford algebra, Clifford analysis, their applications to electrodynamics and quantum theory, and the visualization of geometric vector field structures.

Martin Menzel studied physics and mathematics at the Universität Kaiserslautern from 1985 to 1993. His diploma thesis concerned semiclassical approaches to relativistic quantum mechanics. From 1993 to 1997, he held a position as a research assistant in the Department of Physics at the Universität Kaiserslautern. He finished his doctoral thesis in 1997. The thesis concerned the Clifford-analytic computation of steady electric currents. The support of the current fields was a multiply connected plane region containing anomalies of conductivity. Visualization of the calculated Clifford vector fields was one of the main tasks.

His research interests include numerical algorithms, scientific visualization, vector field topology, Clifford analytic applications to electrodynamics, and quantum mechanics.
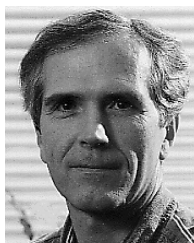
Alyn P. Rockwood completed his BS and MS degrees in mathematics at Brigham Young University and his PhD in applied mathematics and theoretical physics at Cambridge University. He is currently on the computer science faculty at Arizona State University, prior to which he worked in industrial research for 13 years, including positions at Evans and Sutherland, Shape Data, and Silicon Graphics. He will join Power Take Off, Inc., in Longmont, Colorado. His research interests include computer graphics, scientific visualization, and computer-aided geometric design. He will serve as SIGGRAPH '99 papers chair.